Optimization and Control of Pressure Swing Adsorption Processes Under Uncertainty

Harish Khajuria and Efstratios N. Pistikopoulos
Centre for Process System Engineering, Dept. of Chemical Engineering, Imperial College, London SW7 2AZ, U.K.

DOI 10.1002/aic.13783
Published online March 21, 2012 in Wiley Online Library (wileyonlinelibrary.com).

The real-time periodic performance of a pressure swing adsorption (PSA) system strongly depends on the choice of key decision variables and operational considerations such as processing steps and column pressure temporal profiles, making its design and operation a challenging task. This work presents a detailed optimization-based approach for simultaneously incorporating PSA design, operational, and control aspects under the effect of time variant and invariant disturbances. It is applied to a two-bed, six-step PSA system represented by a rigorous mathematical model, where the key optimization objective is to maximize the expected H_2 recovery while achieving a closed loop product H_2 purity of 99.99%, for separating 70% H_2, 30% CH_4 feed. The benefits over sequential design and control approach are shown in terms of closed-loop recovery improvement of more than 3%, while the incorporation of explicit/multiparametric model predictive controllers improves the closed loop performance. © 2012 American Institute of Chemical Engineers *AIChE J,* 59: 120–131, 2013
Keywords: pressure swing adsorption, modeling, dynamic optimization, simultaneous design and control, explicit model-based predictive controller

Introduction

Pressure swing adsorption (PSA) is at the forefront of gas separation technology. Since its commercial inception in late 1950s, PSA technology has evidenced substantial growth in terms of size, versatility, and complexity.[1,2] Modern PSA systems, used widely in the gas separation industry can vary from two adsorbent bed separating air to 16 bed system producing pure hydrogen in excess of 100,000 N m^3/h.[3] In addition to handling multicomponent separation and purification, PSA offers great flexibility at both design and operational stages, requiring careful selection of important decision variables. Further challenges are posed by the fact that the PSA operation is periodic in nature and never attains a true steady state.

The traditional approach for design of such process systems usually uses a two-step, sequential-based approach. In the first step, a typical process synthesis problem is formulated to design a process that satisfies predefined operating requirements.[4–6] Subsequently, to overcome the effect of uncertainty or unforseen scenarios in design operating conditions the system is over-designed using empirical or semiempirical techniques[7–9] such as factor of safety. In the second step, to mitigate the effect of operating disturbances on plant performance, a suitable controller is designed.[10,11] Such a sequential approach is one of the most widely used approaches in the process design community.[4,9,12]

Nonetheless, in the last few decades, the importance of incorporating real-time operability aspects during the design stage itself has been greatly emphasized. Some of the early contributions in this field,[13,14] albeit focussing on simplified linear systems, suggested various analytical tools and indices[15,16] while providing meaningful insights into ways of integrating design and control formulations. A detailed survey of important contributions can be found in Sakizlis et al.,[17] while Table 1 presents some of very recent work in this area. An important trend that has emerged from the past studies is the wide acceptance of optimization-based method[21,22,27–30] and their applications to various systems such as distillation columns,[31–33] CSTRs,[34] and systems represented by reduced models.[26,35] Normally, the application of optimization-based approaches to inherently dynamic and highly nonlinear system like PSA still remains a challenging task. This is the main focus of this study, with particular interest in exploring the effects of PSA decision variables such as the duration of the processing steps on the operability of the system and the appropriate design of its control system.

A key difficulty in the employment of optimization-based approaches for PSA is to overcome the numerical computation and robustness issues encountered while employing a model that mimics the highly nonlinear and inherent dynamic nature of PSA operation. Most of previous studies, as shown in Table 2, have focussed on the acceleration of cyclic steady state (CSS) to minimize the computational load related to the optimization procedures. In this regard, three key methodologies are the complete discretization approach proposed by Nilchan and Pantelides,[37] the unibed formulation from Kumar et al.,[46] and the CSS direct determination approach[40] employed in the work of Jiang et al.[39] In the complete discretization approach,[37] the underlined PDAE-based model is completely discretized both in spatial domain and time domain resulting in a large scale nonlinear

Correspondence concerning this article should be addressed to E. N. Pistikopoulos at e.pistikopoulos@imperial.ac.uk.
Current Address of Harish Khajuria: BASF SE, GTF/ED - L440, 67056 Ludwigshafen, Germany.

Table 1. A Brief Overview of Some Recent Work in the Field of Integrated Design and Control

Authors	IDC Formulation	Case Study	Modeling Details	Controller Details
Asteasuain et al.[18]	Mixed integer dynamic optimization (MIDO) formulation at nominal conditions	Styrene bulk polymerization reactor	DAE	Super structure based MIMO formulation of feedforward-feedback controller
Chawankul et al.[19]	Lumped the capital and operating cost at steady state along with the controller performance cost into a single objective function	Multicomponent distillation column separation	DAE	Robust formulation of SISO control
Asteasuain et al.[20]	Decomposition algorithm[21,22] with outer approximation approach for integer variables and over estimator to simplify the process dynamic feasibility test	Design and control for grade transition of styrene polymerization process	DAE	Super structure based MIMO formulation for feedforward-feedback configuration
Flores-Tlacuahuac and Biegler[23]	ISE treated as objective function, MIDO problem transformed to MINLP by employing finite element method on the state and control variables	CSTR	DAE	Super structure based approach for process and control alternatives
Chawankul et al.[24]	Lumped the capital and operating cost at steady-state along with the controller performance cost into a single objective function. Furthermore, The steady-state model and dynamic models represented by simplified empirical correlations. Model mismatch treated as process uncertainty	Top and bottom purity control for depropanizer column	Empirical correlations deduced from REDFRAC (Aspen PLUS)	Robust formulation for MIMO-based MPC controller
Malcolm et al.[25]	Decomposition algorithm[21,22] with an extra step of steady-state flexibility analysis before the dynamic one to reduce the search space of critical uncertain parameters scenarios. Furthermore, the optimal design and control problem are decoupled with the optimal control problem solved for fixed design. The solution of optimal control subproblem effects the master optimal design problem, if the operation fails in the flexibility tests	Polymerization reactor design and control, and binary column separation	DAE	Fixed controller structure with MIMO formulation
Ricardez-Sandoval et al.[26]	Algorithm based on employing finite impulse response model of the original system at nominal conditions to evaluate the worst case disturbance and critical parametric uncertainty simultaneously. The resulting design is validated by performing closed-loop simulation on the original model	Tennessee Eastmen process	DAE, lumped objective function containing steady-state capital and operating cost with real-time process output variability cost	Fixed controller structure of PI loops

algebraic system of equations, which can be solved by a suitable NLP solver. The successful solution of these equations, however, is very sensitive to the initial guess (of CSS), which is usually hard to obtain. On the other hand, the unibed framework, see also Kumar et al.,[46] for PSA dynamic modeling, makes use of the fact that in a given PSA cycle all beds undergo the same processing steps but with a time lag. Consequently, data storage techniques can be used to store the temporal profiles of all variables to be used later, instead of using another bed. In the direct determination approach, the CSS is posed as a two-point boundary conditions and an update of CSS state is obtained via applying Newton-based method, involving evaluation of the complex sensitivity matrix of the CSS equations.[39,41] It is important to note that all of the CSS acceleration approaches to optimize PSA mainly focuses on predicting the final CSS correctly. The intermediate states toward the CSS evolution are either not evaluated or fictitious in nature, which for the case of control studies are of importance. In our work, the traditional dynamic optimization approach was considered as more suitable for control studies and is employed, in which the model is integrated in time toward a slow but true evolution to the CSS.

The remaining part of the article is organized as follows. The next section outlines the optimization problem with a detailed description of the key challenges in the operation and control of a typical PSA system. The implementation of the employed simultaneous optimization and control strategies is presented next, and applied to a two-bed, six-step PSA system. The results of the simultaneous study are then compared with the traditional sequential approach. An explicit/multiparametric model-based predictive controller (MPC) is also designed and compared to conventional PI controller.

Table 2. A Brief Overview of Important Literature Studies on PSA Optimization

Authors	PSA System	Modeling Details	CSS Acceleration	Optimization Formulation	Objective Function
Smith and Westerberg[36]	H_2—CH_4, and H_2 bulk separation	Very simplified model, comprising time averaged mass and energy balances	Not required	MINLP	Capital and operating costs
Nilchan and Pan-telides[37]	Single-bed RPSA for air separation and two-bed, six-step PSA for N_2 purification from air	Isothermal	Complete discretization of spatial and temporal derivatives	NLP	Average power
Ko et al.[38]	One-bed, Four- step CO_2 sequestration from CO_2—N_2	Constant superficial velocity	CSS evaluated by expressing spatial profile of differential variables in empirical expressions	NLP	Maximize CO_2 and N_2 purity
Jiang et al.[39]	One-bed, three- and six-step air separation	Nonisothermal operation, some state variables profile represented by Lagrangian polynomials	Direct determination approach[40] augmented with a hybrid trust region method for Newton step improvement	NLP, CSS condition posed as a constraint	O_2 recovery and specific work
Jiang et al.[41]	Five-bed, 11-step for H_2 purification from H_2, CH_4, CO, CO_2, and NH_2	Nonisothermal and steady-state momentum balance, bed dispersion neglected	Direct determination approach[39]	NLP[39]	H_2 recovery
Cruz et al.[42]	O_2 production from air; three possible equalization configurations	Nonisothermal operation, model formulated in the dimensionless form to reduce number of variables, employed empirical pressure profile for pressurization/depressurization stages	Not considered	NLP	Recovery and power consumption
Nikolić et al.[43]	H_2 purification from H_2, C_4, CO, and CO_2	Detailed and generic modeling framework[44]	Unibed approach	NLP, repeated optimization for optimal number of beds for predefined PSA cycles	Recovery
Agarwal et al.[45]	Two-bed, four-step PSA, H_2 purification from H_2 and CH_4	Detailed model linear superficial velocity profiles	Performed model reduction employing proper orthogonal collocation	NLP	Recovery

PSA Details and Problem Description

PSA cyclic nature emanates from the simultaneous operation of product purification and adsorbent regeneration steps. Therefore, a multiple bed assembly is used to ensure a constant supply of product, whereas the other beds are in the regeneration mode. During the product purification or adsorption phase, the adsorbent entraps the impurities at high pressure from the incoming feed leaving the pure product coming out at the other end, and during the adsorbent regeneration or desorption phase, these impurities are removed from the column by reducing its pressure in successive steps. The column is then pressurized back to feed pressure making it ready to execute the next cycle. The automatic switching from adsorption to desorption and backforth is performed by the switch valves interconnecting the columns. Furthermore, most of the modern PSA plants have an extra pressure equalization step (between the adsorption step and regeneration step) to properly utilize the high-pressure product for pressurizing other columns.

Modeling details

Figure 1 depicts a graphical overview of the two-bed PSA system under consideration. Each bed is undergoing a cyclic operation comprising six processing steps and contains activated carbon as the adsorbent. Furthermore, it is also assumed that the structure of PSA cycle and sequence of processing steps remains fixed for the purpose of optimization studies. The detailed, first principle based dynamic model of PSA used in this work is an extended version of previous work done by Khajuria and Pistikopoulos.[47] Its main features are described here from Eq. 1 to 6, whereas the boundary conditions are listed in Tables 3 and 4.

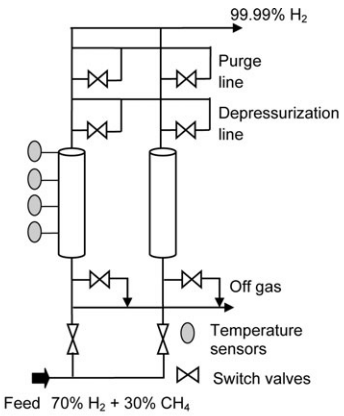

BED1	DEP	BLDN	PURGE	PE	REPRES	FEED
BED 2	PE	REPRES	FEED	DEP	BLDN	PURGE

Figure 1. Two-bed, six-step, multivalve PSA configuration used for this study.

FEED: production step; DEP: cocurrent depressurization; BLDN: counter-current depressurization or blowdown; PURGE: counter-current purge with product; PE: cocurrent pressure equalization; REPRES: cocurrent repressurization with feed.

Mass balance

$$\left(\epsilon_b+(1-\epsilon_b)\epsilon_p\right)\frac{\partial C_i}{\partial t}+\frac{\partial UC_i}{\partial z}+\rho_p(1-\epsilon_b)\frac{\partial \overline{Q_i}}{\partial t}=\epsilon_b D_z\frac{\partial^2 C_i}{\partial z^2} \quad (1)$$

Energy balance

$$\begin{aligned}&\left(\epsilon_b+(1-\epsilon_b)\epsilon_p\right)\sum_{i=1}^{N_{comp}}C_i(C_{p_i}-R)\frac{\partial T}{\partial t}\\&+\rho_p(1-\epsilon_b)\sum_{i=1}^{N_{comp}}\overline{Q_i}(C_{p_i}-R)\frac{\partial T}{\partial t}+U\sum_{i=1}^{N_{comp}}C_iC_{p_i}\frac{\partial T}{\partial z}\\&-\left(\epsilon_b+(1-\epsilon_b)\epsilon_p\right)RT\sum_{i=1}^{N_{comp}}\frac{\partial C_i}{\partial t}+C_{p_s}\rho_p(1-\epsilon_b)\frac{\partial T}{\partial t}\\&-\rho_p(1-\epsilon_b)\sum_{i=1}^{N_{comp}}\frac{\partial \overline{Q_i}}{\partial t}(-\Delta H_i)+\left(\left(1+\frac{\Delta d_w}{D}\right)^2-1\right)\\&\times C_{p_w}\rho_w\frac{\partial T}{\partial t}=\lambda\frac{\partial^2 T}{\partial z^2}\end{aligned} \quad (2)$$

Table 3. Boundary Conditions for the Counter-Current Purge, Counter-Current Pressure Equalization, and Cocurrent Product Repressurization Steps for the Six-Step PSA Cycle

$z=0$	$z=L$
Counter-current purge	
$U=f_{valve}(P,P_{purge},CV_{bldn})$	$CU=-f_{valve}(P_{prod},P,CV_{purge})C_{prod}$
$\frac{\partial C_i}{\partial Z}=0$	$C_i=\frac{P}{RT}\frac{C_{i_{prod}}}{C_{prod}}$
$\frac{\partial T}{\partial Z}=0$	$T=T_{prod}$
Counter-current pressure equalization	
$U=0$	$CU=-f_{valve}(P_{dep},P,CV_{dep})C_{dep}$
$\frac{\partial C_i}{\partial Z}=0$	$C_i=\frac{P}{RT}\frac{C_{i_{dep}}}{C_{dep}}$
$\frac{\partial T}{\partial Z}=0$	$T=T_{dep}$
Cocurrent repressurization with product	
$U=f_{valve}(P_{feed},P,CV_{repres})$	$U=0$
$C_i=\frac{Py_{ifeed}}{RT}$	$\frac{\partial C_i}{\partial Z}=0$
$T=T_{feed}$	$\frac{\partial T}{\partial Z}=0$

Table 4. Modeling Parameters for the Gas-Solid System

Parameter	Value
$K_{LDF_{H2}}$	$15\times 8.89\times 10^{-2}$
ϵ_b	0.4
P_{prod}	7×10^5
C_{p_w}	480
d_p	3
$K_{LDF_{CH4}}$	$15\times 3.96\times 10^{-3}$
ϵ_p	0.566
P_{bldn}	101,325
ρ_w	7900
T^0_{feed}	303.15

Momentum balance

$$-\frac{\partial P}{\partial z}=\frac{150\mu(1-\epsilon_b)^2}{\epsilon_b^3 d_p^3}U+\frac{1.75(1-\epsilon_b)\sum_{i=1}^{N_{comp}}C_iMW_i}{\epsilon_b^3 d_p}|U|U \quad (3)$$

Mass transfer rate

$$\frac{\partial \overline{Q}_i}{\partial t}=K_{LDF_i}(Q_i^*-\overline{Q}_i) \quad (4)$$

Adsorption isotherm

$$\frac{Q_i^*}{Q_i^{max}}=a_iK_iC_iRT\left[1-\sum_{i=1}^{N_{comp}}\left(\frac{Q_i^*}{Q_i^{max}}\right)\right]^{a_i}$$

$$K_i=K_{\infty_i}e^{\frac{-\Delta H_i}{RT}} \quad (5)$$

Pressure transients

$$\begin{aligned}U&=\frac{R}{\epsilon_b\pi D^2}CV\sqrt{1-\left(\frac{P_{low}}{P_{high}}\right)^2}\quad \text{if}\left(\frac{P_{high}}{P_{low}}\right)<P_{critical}\\&=\frac{R}{\epsilon_b\pi D^2}CV\sqrt{1-\left(\frac{1}{P_{critical}}\right)^2}\quad \text{otherwise}\end{aligned}$$

$$\text{where}\qquad P_{critical}=\left(\frac{2}{1+\gamma}\right)^{\frac{\gamma}{1-\gamma}}\gamma=\frac{C_p}{C_p-R} \quad (6)$$

Objective function

A popular objective function for PSA optimization seems to be product recovery (see also Table 2). The main reason toward this trend is its direct relation to the plant operating cost,[42] under the assumption that the PSA feed is already available at high pressure and does not require considerable compression work. In some cases, especially in air separation for O_2 and N_2 production, where the feed (air) is only available at atmospheric pressure, recovery alone is not a true indicator of PSA operating performance, and PSA overall compression work can also play a significant role. On the other hand, the key controller objective is to fast track the closed loop product purity to its desired set point in the event of process disturbances.[47–50] In a PSA operation, as recovery and purity vary in opposite direction[47] with respect to important decision variables, a simultaneous optimization and control strategy appears to be an ideal platform to incorporate the impact of these two conflicting objectives on the real-time PSA performance. In this study, an optimal PSA operational policy and controller configuration is desired, which provides the maximum value of closed loop hydrogen recovery (Eq. 7) while obeying all operational constraints, for the separation of 70% H_2 and 30% CH_4 feed mixture to a product stream of

Table 5. Boundary Conditions for the Feed, Cocurrent Depressurization, and Counter-Current Blowdown Steps for the Six-step PSA Cycle

$Z = 0$	$Z = L$
Feed	
$UA_{bed} = \dot{Q}_{feed}$	$P = P_{prod}$
$C_i = \frac{P y_{ifeed}}{RT}$	$\frac{\partial C_i}{\partial Z} = 0$
$T = T_{feed}$	$\frac{\partial T}{\partial Z} = 0$
Cocurrent depressurization	
$U = 0$	$U = f_{valve}(P, P_{dep}, CV_{dep})$
$\frac{\partial C_i}{\partial Z} = 0$	$\frac{\partial C_i}{\partial Z} = 0$
$\frac{\partial T}{\partial Z} = 0$	$\frac{\partial T}{\partial Z} = 0$
Blowdown	
$U = f_{valve}(P, P_{bldn}, CV_{bldn})$	$U = 0$
$\frac{\partial C_i}{\partial Z} = 0$	$\frac{\partial C_i}{\partial Z} = 0$
$\frac{\partial T}{\partial Z} = 0$	$\frac{\partial T}{\partial Z} = 0$

hydrogen purity (Eq. 8) greater than 99.99%, in the presence of the following disturbances and uncertainty.

1. Feed temperature variations in a sinusoidal fashion with decaying amplitude as defined in Eq. 9.

2. Step increase in PSA feedrate by 0.35 N m^3/h, as defined in Eq. 10.

3. Bounded uncertainty in the hydrogen feed composition, varying from 68 to 73%.

$$\text{Recovery}_{H_2} = \frac{\int_{t_{pres}}^{t_{feed}} C_{H_2} UA_{bed}\Big|_{z=L} dt}{\int_0^{t_{pres}} C_{H_2} UA_{bed}\Big|_{z=0} dt + \int_{t_{pres}}^{t_{feed}} C_{H_2} UA_{bed}\Big|_{z=0} dt} \times 100 \tag{7}$$

$$\text{Purity}_{H_2} = \frac{\int_{t_{pres}}^{t_{feed}} C_{H_2} UA_{bed}\Big|_{z=L} dt}{\sum_{i=1}^{N_{comp}} \int_{t_{pres}}^{t_{feed}} C_i UA_{bed}\Big|_{z=L} dt} \times 100 \tag{8}$$

$$T_{feed}(t) = T_{feed}^0 + 15\ \sin\left(\frac{2\pi t}{10}\right) e^{-t/5} \tag{9}$$

$$\begin{aligned} \dot{Q}_{feed}(t) &= \dot{Q}_{feed}^0 \quad \text{if} \quad t \le 0 \\ &= \dot{Q}_{feed}^0 + 0.35 \quad \text{otherwise} \end{aligned} \tag{10}$$

For providing the controller action, a SISO PI controller (Eq. 11) is assumed, where purity is the control variable and feed step duration is considered as the manipulated variable.[47] Furthermore, integral square error (ISE)[51] of purity, defined in Eq. 12, is treated as the controller performance indicator.

Table 6. Operating Parameters for the PSA CSS Estimation Study

Parameter	Value
CV_{bldn}	0.06504
CV_{pres}	0.006
D	0.157
$\dot{Q}_{feed}$	1.68
t_{dep}	400
CV_{dep}	0.00947
CV_{purge}	5×10^{-4}
L/D	6
t_{feed}	95.1
t_{pres}	30.1

Table 7. Number of PSA Cycles to Achieve Specific CSS Tolerances

	CSS tolerance				
PSA Variable	10^{-5}	10^{-4}	10^{-3}	10^{-2}	10^{-1}
Purity	282	24	1	1	1
Recovery	377	270	166	2	1
$C_{avg}(H_2)$	569	332	233	127	8
$C_{avg}(CH_4)$	339	234	126	25	7
$\overline{Q}_{avg}(H_2)$	179	23	3	1	1
$\overline{Q}_{avg}(CH_4)$	112	66	13	4	1
$Q^*_{avg}(H_2)$	180	23	3	1	1
$Q^*_{avg}(CH_4)$	112	67	13	4	1
T_{avg}	586	343	234	128	4

$$\begin{aligned} t_{feed}(k) &= t_{feed}(k-1) + K_c(e(k) - e(k-1)) + \frac{K_C \Delta t_s}{\tau_I} e(k) \\ e(k) &= (\text{Purity}_{H_2}(k) - 99.99) \times 10^5 \\ t_l &\le t_{feed}(k) \le t_h \\ \Delta t_l &\le \Delta t_{feed}(k) \le \Delta t_h \end{aligned} \tag{11}$$

$$\text{ISE}(t) = 10^5 \int_0^t (\text{Purity}_{H_2}(t) - 99.99)^2 dt \tag{12}$$

CSS definition and time horizon of dynamic optimization problem

In an ideal situation, the time horizon should be set to a large value to allow the PSA system to attain a CSS, which is defined as a state in time where all PSA variables take the same value at the start and the end of a cycle. On the other hand, it is well known that most significant changes in process variables usually occur in the few initial cycles. The number of such cycles, however, depends on the PSA design configuration, its operational policy, and the gas–solid system. To investigate this for the system under consideration (see Tables 5 and 6), a number of numerical experiments are conducted, using a relaxed definition of CSS as shown in Eq. 13, where ε_{CSS} is a small positive number, which plays a critical role in the evaluation of number of cycles required in settling key PSA variables, defined in a lumped fashion, as shown in Eq. 14. Here, yp represents important PSA variables used for monitoring the CSS.

$$e_{CSS}(t) = \text{yp}_{avg}(t) - \text{yp}_{avg}(t - t_{cycletime}) \le \varepsilon_{CSS} \tag{13}$$

$$\text{yp}_{avg} = \int_0^1 \text{yp}(z^*) dz^*; \quad z^* = z/L \tag{14}$$

The results, summarized in Table 7, show that lower values of ε_{CSS} require higher number of PSA cycles for all CSS indicators considered. Furthermore, the hydrogen gas phase molar concentration and bed temperature are the slowest to settle down for a given value of ε_{CSS}. In addition, observing PSA performance indicators, purity, and recovery alone may not be adequate to define CSS, as in this case bed temperature is the slowest to settle down. Based on the above analysis, a value of 50 cycles is selected as the time horizon for PSA dynamic optimization studies.

Decision variables

A number of decision variables related to PSA process design, cycle scheduling, and controller design should be

selected carefully to obtain an optimal performance. The key process design variables considered are the column length, column diameter, and switch valve CVs (ON–OFF operation), while feed rate is included as an operational decision variable. The key PSA schedule variables considered are the time durations of the processing steps of the underlying PSA cycle, as they directly control the extent of related governing physical phenomena, determining the PSA key performance indicators such as recovery, purity, and other operational constraints. Figure 1 shows that out of the time duration variables of the six processing steps, only three can be varied independently to maintain a synchronized PSA operational cycle. It is important to note that the optimal tuning of switch valves, by incorporating their *CV* as decision variable, is crucial to maintain suitable pressure-temporal profiles at the bed ends for varying bed dimensions and step durations (with each iteration of the dynamic optimization solution procedures). For the controller synthesis problem, manipulated variable bias value, controller gain, and integral time are considered as decision variables.

Operational constraints

In the past studies on PSA optimization (Table 2), incorporating hydrogen purity constraint has been considered adequate for the design of an optimal PSA operation. However, only providing purity violation information to the NLP solver can often lead to solutions where other important state variables may take values indicating unrealistic physical behavior during the time horizon of operation. One such consideration is the high value of fluid superficial velocity, especially during the flow reversal processing steps including blowdown and repressurization with feed, which may result in fluidization of the bed. Another important consideration is the sharp rise of bed temperature during the first few PSA cycles in the adsorption stage. Bed temperatures beyond a certain limit can be detrimental to the adsorbent activity and should be avoided. Consequently, such operational constraints are also incorporated in the overall optimization formulation. In this regard, to ensure that the hydrodynamic regime of the PSA is always under packed bed conditions, superficial fluid velocity at bed ends is constrained to be always less than the minimum fluidization velocity.[52] Similarly, temperature at bed locations of $z/L = 0.25, 0.5, 0.75, 1$ is constrained, as shown in Figure 1.

It is important to note the class of constraints discussed with respect to time. Purity acts as an end point constraint, while velocity and temperature violations, on the other hand, should be measured through the complete time horizon of operation. The treatment of path constraints for dynamic optimization problem has been a subject of serious attention, specially for the control vector parameterizations (CVP)[53] approach. The complete discretization approach proposed by Cuthrell and Biegler[54] does not suffer from this drawback, as the discretized path constraints become part of the overall NLP problem. Toward the CVP approach, Feehery and Barton[55] proposed an elegant technique, which involves consuming one DOF from the overall list of available DOFs to satisfy a given path constraint. However, the selection criteria to choose the sacrificing DOF is not unique and relies completely on the user ability to find an appropriate choice. For this particular study, we consider an approach where path constraints are converted into end point constraints by defining violation variables for each path constraint,[56,57] as shown below.

if violation = true **then**

$$\frac{\partial vio\_v}{\partial t} = \text{violation}^2$$

else

$$\frac{\partial vio\_v}{\partial t} = 0$$

end if

From real-time control perspective, it is important to constraint both high and low values of adsorption time (Eq. 11) to achieve a safe and economical operation. Very low values of feed step duration translates to shorter PSA cycles performing loading and unloading of the adsorbent with the impurities at a quicker rate, while significantly enhancing its degradation in the form of wear and tear.[58] Furthermore, this also demands a faster ON and OFF operation of the switch valves, reducing their lifetime, which is directly related to number of switches per unit time. On other hand, long duration feed step can over saturate the bed, because the adsorbent has only a limited capacity for the impurities. In addition to this, large changes in the adsorption time (Δt_{feed}) should also be constrained to avoid over saturation (Δt_{h}) or avoid sudden surge of inflow (Δt_{l}).[47] It is important to note that in general practice, the controller constraints mentioned in Eq. 11 can be treated as constraints in the original NLP problem itself. In this work, the explicit nature of the PI control law is exploited, and an IF–ELSE logic is built to incorporate these equations along with the general PDAE model of PSA. This approach, enhances the convergence rates of the dynamic optimization problem without compromising its rigor.

A Framework for Simultaneous Design and Control Optimization of PSA Systems Under Uncertainty

In general, a system designed at the nominal conditions is liable to fail for small changes of uncertain conditions, in terms of constraint violations and performance degradation. To obtain an optimal PSA design, which is operable under the full range of uncertain parameters, and known time varying disturbances, a rigorous and systematic approach[22,27] is employed. The framework in Figure 2 depicts the employed methodology comprising three main steps.

Step 1: In this step, the uncertain parameter (hydrogen-feed composition) is discretized into a finite number of critical scenarios. As the hydrogen feed composition can vary from 68% to 73%, three critical scenarios are chosen for discretization purposes. The first scenario corresponds to 73% feed composition possibility with probability of 15%, the second scenario corresponds to 68% hydrogen feed composition with 15% probability, while the third represents the nominal case of 70% hydrogen feed composition with 70% probability. Note that the nominal case has been given the highest probability of occurrence, while the upper and lower bounds have been equally treated. The resulting simultaneous design and control optimization formulation is depicted in Eq. 15, where h_{d1} and h_{c1} are the equality constriants representing PSA model and controller description, respectively,

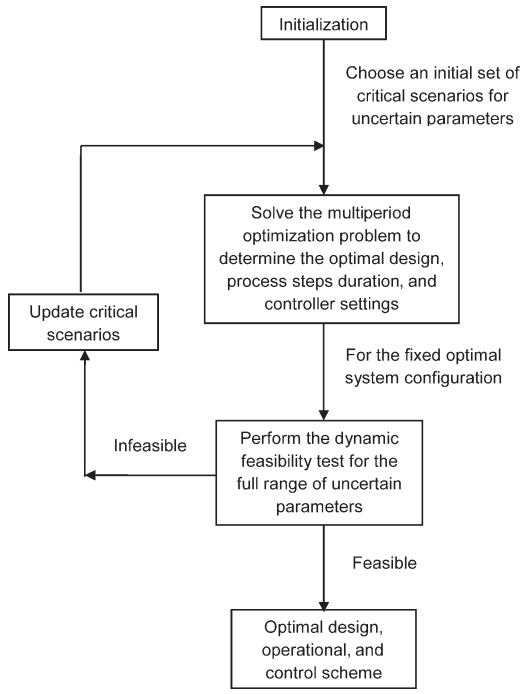

Figure 2. A framework for simultaneous design, operational, and control optimization under uncertainty.

whereas w_{θ_m} denotes the weight of the particular critical scenario m.

$$\max_{d_P,d_c,v,t\in[0,t_f=50\ \text{cyles}]} \text{obj} = \sum_{m=1}^{3} w_{\theta_m} \text{Recovery}_{H_2}(\theta_m)\Big|_{t_f}$$

s.t.

$$\begin{aligned}
h_{d1}(\dot{xd}, xa, d_P, v, \theta_m, t)_m &= 0 \quad m = 1,2,3\\
h_{c1}(\dot{xd}, xa, d_c, v, \theta_m, t)_m &= 0 \quad m = 1,2,3\\
99.99 \le \text{Purity}_{H_2}(\theta_m, t_f)_m &\le 100 \quad m = 1,2,3\\
0 \le \text{ISE}(\theta_m, t_f)_m &\le \varepsilon_c \quad m = 1,2\\
0 \le U^i_{vio}(\theta_m, t_f)_m &\le \varepsilon_d \quad i = 1,2 \quad m = 1,2,3\\
0 \le T^j_{vio}(\theta_m, t_f)_m &\le \varepsilon_d \quad j = 1,2,3,4 \quad m = 1,2,3 \quad (15)
\end{aligned}$$

It should also be noted that ISE is treated as a constraint[59] (instead of being considered as a separate objective function), which makes ε_c a tuning parameter that can be changed to obtain a stable and fast controller response. Here, the values of ε_c and ε_d are fixed at 2 and 10^{-5}, respectively.

Step 2: In this step, the multiperiod dynamic optimization problem formulated in the last step is solved.[60] The resulting optimal decision variables and PSA performance indicators are shown in Table 8. The maximum expected closed loop hydrogen recovery in this case comes out to be around 61% for an expected value of ISE at 1.42.

Step 3: In this step, the dynamic feasibility test[61] is performed to check whether the optimal design and control system obtained in the last step is feasible for the complete range of uncertain parameter. The dynamic feasibility test problem is formulated in Eq. 16. Here, g_l are the set of PSA inequality constraints. If ψ is negative, then the design is feasible for the operating range of uncertain parameter. If it is positive, then the design is infeasible and the critical scenario obtained from the complete solution of Eq. 16 is augmented with the list of critical scenarios described in Step 1, and the whole procedure is repeated till feasibility is achieved.

$$\psi = \max_{l=1,..Ncr} \left[g_l(\theta^*) = \max_{\theta\in[68\%,73\%],t\in[0,t_f=50\ \text{cycles}]} g_l(\theta, t_f) \right] \quad (16)$$

It is important to note that formulation in Eq. 16 assumes that there are no time variant decision variables in the optimization problem. The value of ψ (Eq. 16) for the current design and control configuration comes out to be -7.5×10^{-5}, with purity lower bound as the limiting constraint. As this is a negative value, the optimal PSA design obtained here is feasible and the algorithm terminates.

Computational Results and Discussions

For the PSA system shown in Figure 1, the resulting design and control configuration obtained by the employment of the methodology mentioned in previous section is shown in Table 8, whereas the corresponding computational statistics are outlined in Table 9. Note that for the two-bed PSA system under consideration, the total CPU time to solve the full optimization problem is around 9.2 h. Table 8 also depicts the optimal values of key degrees of freedom related to process design, operation, and controller design of the PSA system. In particular, the following remarks can be made:

1. The duration of feed step is the largest as compared to other two steps. For the two-bed, six-step PSA cycle under consideration, where feed is provided in only one step (per bed) and then discontinued, this result seems quite logical and can be attributed to the fact that it is during the feed step that actual recovery of product happens, which the optimizer attempts to maximize.

2. The system spends least amount of time in the pressurization/blowdown stage. This result appears to be in order with the fact that for the given PSA cycle, the system would like to quickly repressurize the column (from feed) in an attempt to minimize the impurity intake during this time, as well quickly depressurize (blowdown) the column to minimize the product losses in the off gas.

To further assess the design performance, dynamic simulations are performed[60] with the optimal PSA system listed in

Table 8. Optimal Decision Variables, Their Upper and Lower Bounds and Optimal Performance Variables for PSA Optimization Under Uncertainty Study

Decision Variable	LB	UB	Value
Process design			
CV_{bldn}	0.065	1	0.0652
CV_{dep}	0.01	1	0.010
CV_{repres}	0.06	1	0.06
CV_{purge}	7.7×10^{-5}	5×10^{-4}	5×10^{-4}
D	0.05	0.5	0.1598
L/D	2	6	6
Operational			
$Qdot;_{feed}$	0.5	1.7	1.699
t_{dep}	15	150	93.432
t_{repres}	30	150	37.83
Controller design			
$t_{feed}(t_0)$	60	400	336.211
Kc	0.001	100	0.1842
τ_I	0.001	10^5	4.049
θ	Recovery_{H_2}	Purity_{H_2}	ISE
Performance variables for multiperiod design			
68%	60.86%	99.99%	1.571
70%	60.933%	99.99%	1.41
73%	61.01%	99.99%	1.3
Expected values	60.933	99.99%	1.418

Table 9. Solver and Convergence Statistics for the PSA Multiperiod Optimization Solution[60] (Table 8)

Parameter	Value
Number of axial nodes	40
Discretization scheme	CFDM
DAE solver absolute and relative convergence tolerance	10^{-6}
Number of NLP iterations	8
Number of NLP line searches	14
NLP solver convergence tolerance	6.4×10^{-4}
CPU time (s)	32,897
Fraction of CPU time spent on sensitivity integration (%)	58
Machine details	Intel Xeon E5450 @ 3.00 GHz

Table 8 and feed composition parameter fixed at 70% value. In the following, this design configuration will be referred to as nominal PSA design.

The spatial variation of gas phase concentration of impurity component at the end of each processing step at CSS is shown in Figure 3. Figures 3 and 4, in particular displays the impurity adsorption and desorption dynamics for each PSA process step. During the feed mode, 20% of bed (toward the feed end) is almost saturated with methane. By the end of depressurization step, the impurity front moves slightly forward as the product end is now open to pressurize the other column undergoing pressure equalization. This behavior also emphasizes the importance of each processing step duration. For example, a little extra long depressurization step can lead to impurity leaving the product end to the clean product end of the other column. On the other hand, a shorter duration step will not completely utilize the high-purity product available at high pressure, and instead leaving with the off gas in the next step (blowdown). Blowdown step marks the start of the adsorbent regeneration stage, as the methane concentration falls sharply. By the end of purge step, the impurity level in the bed has reached its minimum level. During the pressure equalization by product and pressurization by feed step, the column is pressurized back to the feed pressure. It is important to note that substantial adsorption in the bed can happen during the repressurization with feed step. This demands a fast repressurization step, where the gas phase concentration increases much faster than the solid phase concentration. A closer comparison of Figures 3 and 4 confirms this behavior where it can be seen that the area under the curve

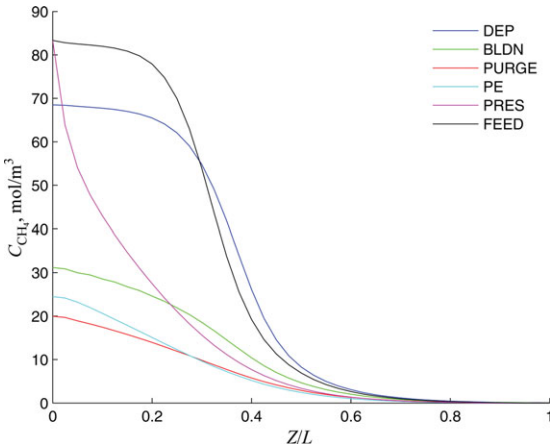

Figure 3. Axial distribution of gas-phase methane concentration at CSS.

[Color figure can be viewed in the online issue, which is available at wileyonlinelibrary.com.]

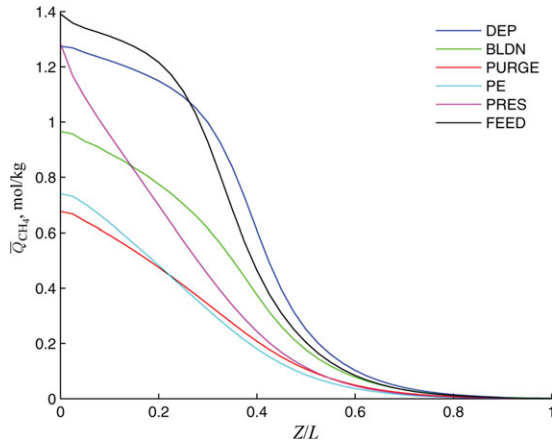

Figure 4. Axial distribution of $\overline{Q}_{CH_4}$ at CSS.

[Color figure can be viewed in the online issue, which is available at wileyonlinelibrary.com.]

rises much sharply for C_{CH_4} than $\overline{Q}_{CH_4}$, while moving from PE step to PRES step. In fact detailed calculations performed shows that the $C_{CH_{4avg}}$ (Eq. 14) increases twice as fast as $\overline{Q}_{CH_{4avg}}$.

Figure 5 depicts the complex interaction between the pressure swings, and the corresponding temperature swings for one complete PSA cycle for the first bed. From this plot, it can be deduced that the temperature swing cycle is much slower to settle down as compared to pressure swing and also has an unfavorable effect on the PSA performance due to the temperature rise during the adsorption stages and drop during the desorption stages. Furthermore, it also reveals that the repressurization at CSS is much faster than the blowdown, as the bed pressure at the end of blowdown stage has not reached the lowest pressure possible.

Comparisons with a Sequential Strategy

Table 10 compares the optimal PSA operational configurations obtained from the application of sequential and the simultaneous approach while assuming perfect certainty in feed composition at $y_{H_2} = 70\%$.

The results shows that if the ISE is kept around the same value obtained from the sequential approach, the simultaneous approach provides better closed loop recovery. In this case, the actual recovery possible is 61.638% which is almost 3% higher (on relative basis) than the recovery obtained from the sequential approach. When comparing the results in different

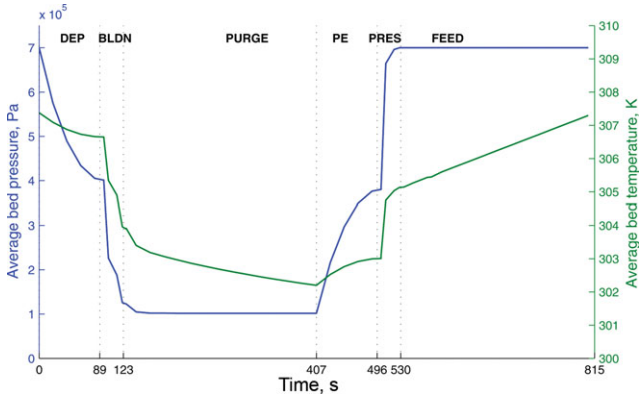

Figure 5. Time evolution of pressure swing and the associated temperature swing over a PSA cycle at the optimal conditions.

[Color figure can be viewed in the online issue, which is available at wileyonlinelibrary.com.]

Table 10. Comparison of Optimal PSA Systems Obtained from Sequential and Simultaneous Approach

	Sequential Approach		Simultaneous Approach	
	Process Synthesis (Maximize $Recovery_{H_2}$)	PI Controller Design (Minimize ISE)	($\varepsilon_c = 2.5$)	($\varepsilon_c = 1$)
Decision variable				
$CV_{blowdown}$	0.06502		0.06532	0.065
CV_{dep}	0.0102		0.01	0.01
CV_{repres}	0.06		0.06	0.06
CV_{purge}		5×10^{-4}	5×10^{-4}	5×10^{-4}
D	0.1574		0.16	0.15936
L/D	6		6	6
$\dot{Q}^0_{feed}$	1.698		1.7	1.7
t_{dep}	86.58		97.124	92.3317
t_{feed}	399.99		311.051	366.118
t_{repres}	30.15		38.273	31.358
Kc		0.55323	0.061	0.336
τ_I		7.64	1.06	7.45
Performance variables				
$Recovery_{H_2}$	62.98	59.88	61.638	60.82
$Purity_{H_2}$	99.99	99.99	99.99	99.99
ISE		2.2	2.45	0.99

columns of Table 10, it should be noted that t_{feed} is the duration of the feed step for the sequential analysis, while it is the initial value (bias value) of PI control law for the simultaneous optimization studies. It is also evident from the results, that simultaneous approach predicts a design that is marginally bigger in size with respect to both diameter and length (as L/D ratio is unchanged). The largest change is observed in the step durations of the PSA cycle, as the simultaneous optimization-based approach predicts higher time duration for all processing steps at optimal CSS conditions in comparison to the sequential approach. These observations suggests that the simultaneous approach predicts a bigger and slower PSA system in

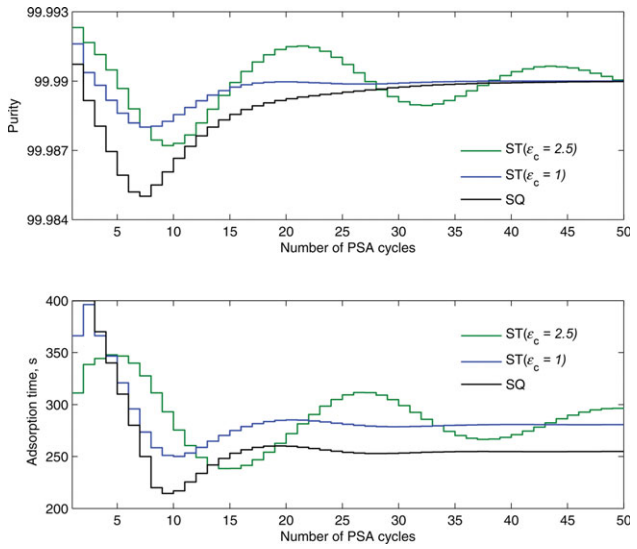

Figure 6. Comparison of closed-loop controller performance for various optimal PSA systems and controller settings.

ST: simultaneous approach, SQ: sequential approach. [Color figure can be viewed in the online issue, which is available at wileyonlinelibrary.com.]

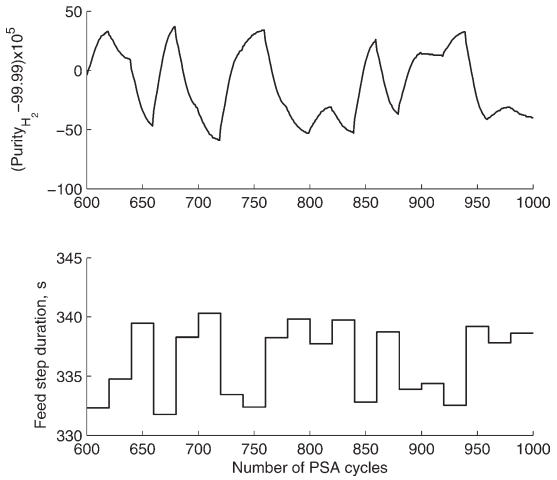

Figure 7. Purity response corresponding to the random variations in the manipulated variable.

an attempt to effectively handle specified disturbances, while also increasing the closed loop recovery at CSS conditions.

The resulting controller responses are compared in Figure 6. It shows that with the sequential design and control (SQDC) approach, the product purity goes to very low values of 99.985% in the first few cycles. In contrast to this, the simultaneous design and control (SDC) formulation provides better purity response. For the case of ISE = 2.5, the purity response is somewhat oscillatory, although very tightly bounded to the set point. It can also be seen that lowering ε_c improves the purity response a lot in terms of reducing the oscillatory effect. However, this improvement is achieved at the price of slight reduction in product recovery, albeit the product recovery level is still higher than the SQDC case.

Explicit/Multiparametric MPC for PSA

At this point, it appears worthwhile to investigate how a MPC controller would behave for the design and operational configuration obtained from the multiperiod optimization. To further investigate this, an explicit/multiparametric MPC controller is built for the nominal PSA design case (Table 8).

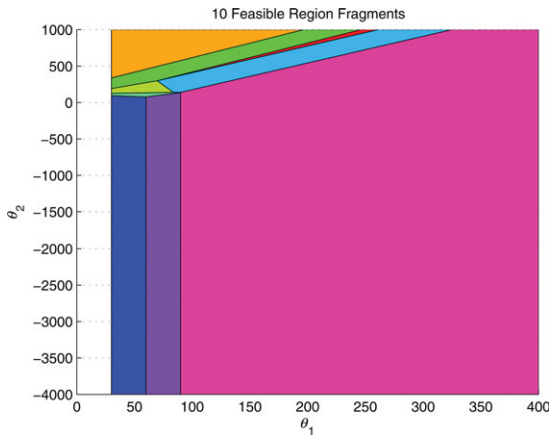

Figure 8. Two-dimensional projection of 101 critical region polyhedra corresponding to the reduced state space model, [x_1,.. x_5 = 0, $t_{feed}(k) = u = \theta_1$, ($Purity_{H_2}$ − 99.99) × $10^5 = y = \theta_2$, y_{set} = 0].

[Color figure can be viewed in the online issue, which is available at wileyonlinelibrary.com.]

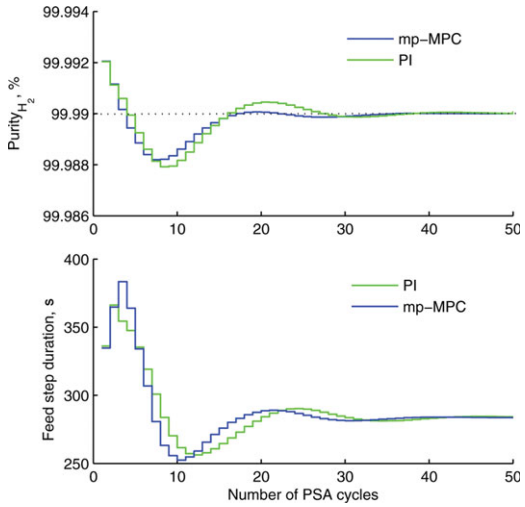

Figure 9. Comparison of closed-loop performance for the PI and mp-MPC controller.

[Color figure can be viewed in the online issue, which is available at wileyonlinelibrary.com.]

MPC in general, is an advanced control methodology specially suitable for highly complex, interconnected dynamic systems. In contrast to a standard PID-based controller, MPC provides optimal control action by taking into account system's dynamic behavior and operational constraints.[62–65] It is based on receding horizon philosophy, where the current plant state and output variables, along with a suitable plant model, are utilized to calculate the future sequence of optimal input variables, via solving an online optimization problem. Recent advances made in the field of multiparametric programming now makes it possible to obtain the governing MPC control law beforehand, or "offline",[66] leading to reduced online computations and other economic benefits.[67–69]

As, the large-scale PSA model developed is not directly suitable for model-based controller design, a system identification step[70–73] is performed to identify a much simpler, preferably linear model relating the control variable with the manipulated variable to reasonable accuracy. The identification procedure followed in this study involves conducting dynamic simulations on the PDAE model, perturbed by a random pulse of input (feed step duration) disturbance, to ensure that the PSA system is excited "persistently"[70,72] over a large frequency band (of interest), in the open loop environment. The resulting input–output response data (Figure 7) is used within the MATLAB system identification toolbox to identify the best fit linear parametric model. The best fit is achieved for a Fifth-order state space model (Appendix) with a mismatch of less than 5% from the PDAE model response.

$$\min_u Z = \sum_{k=1}^{N-1} (y(k) - y^r(k))^T (y(k) - y^r(k)) + \sum_{k=0}^{M-1} \Delta u(k)^T RU \Delta u(k)$$

s.t.

$$\begin{aligned} x(k+1) &= Ax(k) + bu(k) \\ y(k) &= cx(k) + e(k) \\ u_l \le u(k) &\le u_h \\ \Delta u_l \le \Delta u(k) &\le \Delta u_h \\ y(k) &\le 1 \end{aligned} \tag{17}$$

A MPC incorporating all controller constraints (Eq. 11) in an optimization framework is formulated in Eq. (17). The complete problem is set up in the POP toolbox environment[74] and involves eight parameters. The best value for RU is obtained by perturbing the original rigorous PSA model with time varying disturbances (Eqs. 9 and 10) and performing closed loop simulations. This procedure yields a value of $RU = 1$ with 101 critical regions. Figure 8 shows a two-dimensional projection of the multidimensional polyhedra, while the resulting closed loop performance is shown in Figure 9 along with the PI control performance. The comparison shows that the mp-MPC controller provides much more robust response in terms of less oscillatory behavior in purity response. It is also important to note that the PI controller in this case is a special one, as it considers all the system constraints, in a fashion similar to a mp-MPC controller. This appears to be main reason for the observation that the mp-MPC controller performance is not strikingly different from the PI case. The predictive power of the mp-MPC however, using the system dynamic model, seems to be the key feature for its slightly superior performance than the PI case.

Conclusions and Future Directions

This work presents a detailed study for the simultaneous design, operation and control of a PSA system following a rigorous and systematic framework-based optimization approach while utilizing a detailed mechanistic mathematical model. Important PSA operational challenges, constraints, and objectives are discussed in detail and incorporated in the mathematical framework. The best closed loop recovery obtained for the PSA system under consideration is around 61%, while handling multiple disturbance scenarios. The benefits of PSA design based on this approach as compared to the traditional sequential approach are shown in terms of improvement in closed loop recovery by almost 3% and better purity response. It is also found that the improved design is slightly bigger in size with slower PSA cycles. Furthermore, a mp-MPC is also designed to observe any further benefits related to the model-based controller. The results show improvement, albeit marginal, in the closed loop response with respect to the optimized PI controller considered in the study.

Due to PSA inherent feature of achieving only a CSS, detailed and computationally challenging, dynamic optimization procedures has to be used for design purposes in this study. This is in sharp contrast to other dynamic processes, where at steady state the time derivatives approaches zero and steady state optimization can be effectively employed without the need of calculating the CPU intensive, model sensitivities with respect to the decision variables through out the time horizon of operation. Table 9 shows that more than half of the CPU time is spent in the sensitivity calculations. A possible way to accelerate the PSA optimization procedure is to approximate sensitivity information only at the end (CSS) or toward the end. Furthermore, bypassing the sensitivities for most part of the time horizon would significantly enhance the robustness of the numerical optimization procedures, without compromising its rigorousness.

Another area of improvement is to incorporate the controller stability and robustness features in the Step 2 of the PSA optimization under uncertainty procedure itself. The combination of ISE and dynamic feasibility test, as shown in this study appears to be an efficient methodology to handle time varying and invariant disturbances. In this context, it is important to note

that ISE as a choice of controller performance indicator, especially for MIMO[75] systems, does not cover all aspects of a controller response including the stability issue. In principle, solution of the controller synthesis problem can result in an optimal input trajectory, which is oscillatory in nature. Embedding controller stability and robustness measures (in the form of additional constraints) in the controller synthesis formulation, though is expected to complicate the overall design methodology, should be investigated to observe any benefits in terms of design with superior operability.

Acknowledgments

Financial support from the Royal Commission for the Exhibition of 1851, ParOS Ltd., EU project HY2SEPS (contract number: 019887), EPSRC (EP/G059071/1, EP/I014640/1), and KAUST is sincerely acknowledged. The authors also thank HY2SEPS for kindly providing the experimental data for the gas–solid system.

Notation

Roman letters

A_{bed} = bed area, m^2
C = gas phase molar concentration, mol/m^3
C_p = gas phase molar specific heat at constant pressure, J/mol K
C_{p_w} = column wall specific heat, J/kg K
d_p = particle diameter, mm
d_P = process design decision variables
d_c = controller design decision variables
D = bed diameter, m
D_z = axial mass transfer coefficient, m^2/s
K_{LDF} = LDF rate constant, 1/s
k = sampling instant
Kc = proportional gain for PI controller
L = bed length, m
P = bed pressure, Pa
$\dot{Q}$ = volumetric feed flow rate, N m^3/h
Q^* = adsorbed phase concentration in equilibrium with bulk gas, mol/kg
$\overline{Q}$ = volume averaged adsorbed phase concentration, mol/kg
Q^{max} = maximum adsorbed phase concentration in equilibrium with bulk gas, mol/kg
R = ideal gas constant, J/mol K
RU = weight constant for the MPC ΔU term
t = time, s
Δt_s = sampling interval
T = gas or solid phase temperature, K
u = controller output or process input variables
U = superficial velocity, m/s
v = operational decision variables
$\dot{x}d$ = differential variables
xa = algebraic variables
y = controlled or process output variable

Greek symbols

ϵ_b = bulk phase porosity
ϵ_p = Particle phase porosity
ε_d = design tolerance
ε_c = control tolerance
ε_{CSS} = CSS tolerance
θ = parametric uncertainty
λ = axial heat transfer coefficient, W/m K
ρ_w = column wall density, kg/m^3
τ_I = integral time constant for PI controller

Subscripts

i = gaseous species
bldn = blowdown step of PSA cycle
dep = depressurization step of PSA cycle
f = final value
feed = feed step of PSA cycle or feed conditions
purge = purge step of PSA cycle
repress = repressurization step of PSA cycle
s = solid phase property

Literature Cited

1. Ruthven DM, Farooq S, Knaebel KS. *Pressure Swing Adsorption*. Wiley-VCH, 1994.
2. Yang RT. *Gas Separation by Adsorption Processes*. Imperial College Press; 1997.
3. Whysall M, Wagemans LJM. Very large-scale pressure swing adsorption processes, 2001. U.S. Patent Number 6210466B1.
4. Seider WD, Seader J, Lewin DR. *Product and Process Design Principles*. 2nd ed. Wiley, 1999.
5. Seader JD. *Separation Process Principles*. Wiley, 1998.
6. Douglas JM. *Conceptual Design of Chemical Processes*. McGraw-Hill, 1988.
7. Walas SM. *Chemical Process Equipment: Selection and Design*. Butterworth-Heinemann Ltd. 1995.
8. Ulrich GD. *A Guide to Chemical Engineering Process Design and Economics*. Wiley, 1984.
9. Perry RH, Green DW, Maloney JO, editors. *Perry's Chemical Engineers' Handbook*. McGraw-Hill, 1997.
10. Ogata K. *Modern Control Engineering*. Prentice Hall, 1997.
11. Lipták BG. *Instrument Engineers' Handbook. Process Control and Optimization*, Vol. 2. CRC Press, 2006.
12. Georgis D, Jogwar SS, Almansoori AS, Daoutidis P. Design and control of energy integrated sofc systems for in situ hydrogen production and power generation. *Comput Chem Eng*. 2011;35(9):1691–1704.
13. Lenhoff AM, Morari M. Design of resilient processing plants—I Process design under consideration of dynamic aspects. *Chem Eng Sci*. 1982;37(2):245–258.
14. Morari M. Design of resilient processing plants—III: a general framework for the assessment of dynamic resilience. *Chem Eng Sci*. 1983;38(11):1881–1891.
15. Skogestad S, Morari M. Effect of disturbance directions on closedloop performance. *Ind Eng Chem Res*. 1987;26(10):2029–2035.
16. Palazoglu A, Arkun Y. A multiobjective approach to design chemical plants with robust dynamic operability characteristics. *Comput Chem Eng*. 1986;10(6):567–575.
17. Sakizlis V, Perkins JD, Pistikopoulos EN. Recent advances in optimization-based simultaneous process and control design. *Comput Chem Eng*. 2004;28(10):2069–2086.
18. Asteasuain M, Brandolin A, Sarmoria C, Bandoni A. Simultaneous design and control of a semibatch styrene polymerization reactor. *Ind Eng Chem Res*. 2004;43(17):5233–5247.
19. Chawankul N, Budman H, Douglas P. The integration of design and control: IMC control and robustness. *Comput Chem Eng*. 2005;29(2):261–271.
20. Asteasuain M, Sarmoria C, Brandolin A, Bandoni A. Integration of control aspects and uncertainty in the process design of polymerization reactors. *Chem Eng J*. 2007;131(1–3):135–144.
21. Perkins JD, Walsh SPK. Optimization as a tool for design/control integration. *Comput Chem Eng*. 1996;20(4):315–323.
22. Mohideen MJ, Perkins JD, Pistikopoulos EN. Optimal design of dynamic systems under uncertainty. *AIChE J*. 1996;42(8):2251–2272.
23. Flores-Tlacuahuac A, Biegler LT. Simultaneous mixed-integer dynamic optimization for integrated design and control. *Comput Chem Eng* 2007;31(5–6):588–600.
24. Chawankul N, Sandoval LR, Budman H, Douglas PL. Integration of design and control: a robust control approach using MPC. *Can J Chem Eng*. 2007;85(4):433–446.
25. Malcolm A, Polan J, Zhang L, Ogunnaike BA, Linninger AA. Integrating systems design and control using dynamic flexibility analysis. *AIChE J*. 2007;53(8):2048–2061.
26. Ricardez-Sandoval L, Douglas P, Budman H. A methodology for the simultaneous design and control of large-scale systems under process parameter uncertainty. *Comput Chem Eng*. 2011;35(2):307–318.
27. Bansal V, Perkins J, Pistikopoulos E, Ross R, van Schijndel J. Simultaneous design and control optimisation under uncertainty. *Comput Chem Eng*. 2000;24(2–7):261–266.
28. Bansal V, Sakizlis V, Ross R, Perkins JD, Pistikopoulos EN. New algorithms for mixed-integer dynamic optimization. *Comput Chem Eng*. 2003;27(5):647–668.
29. Moon J, Kim S, Linninger AA. Integrated design and control under uncertainty: embedded control optimization for plantwide processes. *Comput Chem Eng*. 2011;35(9):1718–1724.
30. Varigonda S, Georgiou T, Daoutidis P. Numerical solution of the optimal periodic control problem using differential flatness. *IEEE Trans Automatic Control*. 2004;49(2):271–275.
31. Bansal V, Ross R, Perkins JD, Pistikopoulos EN. The interactions of design and control: double-effect distillation. *J Process Control*. 2000;10(2–3):219–227.

32. Bansal V, Perkins JD, Pistikopoulos EN. A case study in simultaneous design and control using rigorous, mixed-integer dynamic optimization models. *Ind Eng Chem Res*. 2002;41(4):760–778.
33. Sakizlis V, Perkins JD, Pistikopoulos EN. Parametric controllers in simultaneous process and control design optimization. *Ind Eng Chem Res*. 2003;42(20):4545–4563.
34. Hamid MKA, Sin G, Gani R. Integration of process design and controller design for chemical processes using model-based methodology. *Comput Chem Eng*. 2010;34(5):683–699.
35. Ricardez-Sandoval LA, Budman HM, Douglas PL. Simultaneous design and control: a new approach and comparisons with existing methodologies. *Ind Eng Chem Res*. 2010;49(6):2822–2833.
36. Smith OJ, Westerberg AW. The optimal design of pressure swing adsorption systems. *Chem Eng Sci*. 1991;46(12):2967–2976.
37. Nilchan S, Pantelides C. On the optimisation of periodic adsorption processes. *Adsorption* 1998;4(2):113–147.
38. Ko D, Siriwardane R, Biegler LT. Optimization of a pressure-swing adsorption process using zeolite 13x for CO_2 sequestration. *Ind Eng Chem Res*. 2003;42(2):339–348.
39. Jiang L, Biegler LT, Fox VG. Simulation and optimization of pressure-swing adsorption systems for air separation. *AIChE J*. 2003; 49(5):1140–1157.
40. Ding Y, LeVan MD. Periodic states of adsorption cycles. III. convergence acceleration for direct determination. *Chem Eng Sci*. 2001;56(17):5217–5230.
41. Jiang L, Fox VG, Biegler LT. Simulation and optimal design of multiple-bed pressure swing adsorption systems. *AIChE J*. 2004;50(11):2904–2917.
42. Cruz P, Magalhes FD, Mendes A. On the optimization of cyclic adsorption separation processes. *AIChE J*. 2005;51(5):1377–1395.
43. Nikolić D, Kikkinides ES, Georgiadis MC. Optimization of multibed pressure swing adsorption processes. *Ind Eng Chem Res*. 2009; 48(11):5388–5398.
44. Nikolic D, Giovanoglou A, Georgiadis MC, Kikkinides ES. Generic modeling framework for gas separations using multibed pressure swing adsorption processes. *Ind Eng Chem Res*. 2008;47(9):3156–3169.
45. Agarwal A, Biegler LT, Zitney SE. Simulation and optimization of pressure swing adsorption systems using reduced-order modeling. *Ind Eng Chem Res*. 2009;48(5):2327–2343.
46. Kumar R, Fox VG, Hartzog DG, Larson RE, Chen YC, Houghton PA, Naheiri T. A versatile process simulator for adsorptive separations. *Chem Eng Sci*. 1994;49(18):3115–3125.
47. Khajuria H, Pistikopoulos EN. Dynamic modeling and explicit/multi-parametric mpc control of pressure swing adsorption systems. *J Process Control*. 2011;21(1):151–163.
48. Bitzer M, Zeitz M. Design of a nonlinear distributed parameter observer for a pressure swing adsorption plant. *J Process Control*. 2002;12(4):533–543.
49. Bitzer M. Model-based nonlinear tracking control of pressure swing adsorption plants. In: Meurer T, Graichen K, Gilles ED, editors. *Control and Observer Design for Nonlinear Finite and Infinite Dimensional Systems*; Vol. 322/2005 of *Lecture Notes in Control and Information Sciences*. Berlin/Heidelberg: Springer, 2005:403–418.
50. Khajuria H, Pistikopoulos EN. An explicit/multi-parametric controller design for pressure swing adsorption system. In: Kothare M, Tade M, Wouwer AV, Smets I, editors. *Proceedings of the 9th International Symposium on Dynamics and Control of Process Systems (DYCOPS 2010)*, Leuven, Belgium, 2010:192–197.
51. Seborg DE, Edgar TF, Mellichamp DA. *Process Dynamics and Control*. Wiley, 1989.
52. Wen CY, Yu YH. A generalized method for predicting the minimum fluidization velocity. *AIChE J*. 1966;12(3):610–612.
53. Vassiliadis VS, Sargent RWH, Pantelides CC. Solution of a class of multistage dynamic optimization problems. 1. problems without path constraints. *Ind Eng Chem Res*. 1994;33(9):2111–2122.
54. Cuthrell JE, Biegler LT. On the optimization of differential-algebraic process systems. *AIChE J*. 1987;33(8):1257–1270.
55. Feehery WF, Barton PI. Dynamic optimization with state variable path constraints. *Comput Chem Eng*. 1998;22(9):1241–1256.
56. Vassiliadis VS, Sargent RWH, Pantelides CC. Solution of a class of multistage dynamic optimization problems. 2. Problems with path constraints. *Ind Eng Chem Res*. 1994;33(9):2123–2133.
57. Barton PI, Banga JR, Galn S. Optimization of hybrid discrete/continuous dynamic systems. *Comput Chem Eng*. 2000;24(9–10):2171–2182.
58. Stewart AB, Henzler GW, Leavitt FW, Notaro F, Kane MS. Psa apparatus and process using adsorbent mixtures, 2000. U.S. Patent Number US006027548A.
59. Luyben M, Floudas C. Analyzing the interaction of design and control—1. a multiobjective framework and application to binary distillation synthesis. *Comput Chem Eng*. 1994;18(10):933–969.
60. Process Systems Enterprise, Ltd. gPROMS Model Developer Guide., 2008. Available at: http://www.psenterprise.com/gproms/index.html.
61. Dimitriadis VD, Pistikopoulos EN. Flexibility analysis of dynamic systems. *Ind Eng Chem Res*. 1995;34(12):4451–4462.
62. Qin SJ, Badgwell TA. A survey of industrial model predictive control technology. *Control Eng Pract*. 2003;11(7):733–764.
63. Rawlings J. Tutorial overview of model predictive control. *IEEE Control Syst Mag*. 2000;20(3):38–52.
64. Maciejowski JM. *Predictive Control with Constraints*. Pearson Education, 2002.
65. Rawlings JB, Mayne DQ. *Model Predictive Control: Theory and Design*. Nob Hill Publishing, 2009.
66. Pistikopoulos EN, Dua V, Bozinis NA, Bemporad A, Morari M. Online optimization via o.-line parametric optimization tools. *Comput Chem Eng*. 2000;24(2–7):183–188.
67. Pistikopoulos EN. Perspectives in multiparametric programming and explicit model predictive control. *AIChE J*. 2009;55(8):1918–1925.
68. Pistikopoulos EN, Georgiadis MC, Dua V. *Multi-Parametric Model-Based Control: Theory and Applications*, Vol. 2. Wiley-VCH, 2007.
69. Pistikopoulos EN, Georgiadis MC, Dua V. *Mulit-Parametric Programming: Theory, Algorithms, and Applications*, Vol. 1. Wiley-VCH, 2007.
70. Söderström T, Stoica P. *System Indentification*. Prentice Hall, 1989.
71. Ljung L. *Modeling of Dynamic Systems*. PTR Prentice Hall, 1994.
72. Ljung L. *System Identi.cation: Theory for the User*. PTR Prentice Hall, 1987.
73. Zhu Y. *Multivariable System Identification for Process Control*. Elsevier/Pergamon, 2001.
74. Parametric optimization solutions (ParOS) Ltd. Parametric Optimization Programming (POP) Toolbox. Available at: www.parostech.-co.uk; 2009.
75. Yuan Z, Chen B, Zhao J. An overview on controllability analysis of chemical processes. *AIChE J*. 2011;57(5):1185–1201.

Appendix: Reduced State Space Model Derived From the System Identification Procedures for MPC Control

Reduce model form

$$\begin{aligned} x(k+1) &= Ax(k) + bu(k) \\ y(k) &= cx(k) \end{aligned} \tag{A1}$$

$$\boldsymbol{A} = \begin{bmatrix} 0.99880 & 0.10001 & 0.00169 & -0.00164 & -0.00034 \\ -0.03130 & 0.96193 & 0.03544 & -0.04382 & 0.03722 \\ 0.13610 & -0.18581 & 0.75535 & 0.13967 & 0.13908 \\ 0.04925 & -0.01173 & -0.36065 & 0.79947 & 0.49361 \\ 0.06341 & -0.08066 & -0.29210 & -0.36313 & 0.02829 \end{bmatrix}$$

$$b = \begin{bmatrix} 0.00523 \\ -0.03004 \\ -0.01797 \\ -0.27463 \\ 0.15461 \end{bmatrix}$$

$$c = \begin{bmatrix} -503.883 & -27.586 & -0.528 & 1.038 & -0.307 \end{bmatrix}$$

Manuscript received Sept. 14, 2011, and revision received Feb. 1, 2012.